
Hierarchically Clustered PCA, LLE, and CCA via a Convex Clustering Penalty

Amanda M. Buch^{1,2} Conor Liston^{1,3} Logan Groseknick¹

Abstract

We introduce an unsupervised learning approach that combines the truncated singular value decomposition with convex clustering to estimate within-cluster directions of maximum variance/covariance (in the variables) while simultaneously hierarchically clustering (on observations). In contrast to previous work on joint clustering and embedding, our approach has a straightforward formulation, is readily scalable via distributed optimization, and admits a direct interpretation as hierarchically clustered principal component analysis (PCA), hierarchically clustered locally linear embedding (LLE), or hierarchically clustered canonical correlation analysis (CCA). Through numerical experiments and real-world examples relevant to precision medicine, we show that our approach outperforms traditional and contemporary clustering methods on both underdetermined problems ($p \gg N$ with tens of observations) and on large datasets (e.g., $N = 100,000$) while yielding interpretable dendrograms of hierarchical per-cluster principal components or canonical variates.

1. Introduction

Explainable clustering across samples or individuals is important in countless real-world applications. In medical diagnoses, interpretable clustering of patients into distinct subtypes is increasingly important for personalized treatment (Sørliie et al., 2001; Santos et al., 2015; Drysdale et al., 2017; Singh & Pandey, 2018; Qian et al., 2019; Bonacchi et al., 2020; Bishop et al., 2022). Due to the curse of dimensionality, similarity metrics (and thus clustering algorithm

outcomes) degrade in high dimensions (i.e. the “ $p > N$ ” or “large dimensional limit” setting common in medical imaging, genomics, and multiomics, where we have p correlated variables and a limited number of observations N on the same scale or smaller than p). As a result, it is popular to use a two-stage procedure where high dimensional data are first embedded into a low-rank representation, and then clustered in this reduced dimension space. The mapping to the low-rank space (e.g., principal component loadings) are then often used to explain which variables are important (e.g., which differences in brain regions or genes relate to cluster differences (Drysdale et al., 2017; Ciortan & Defrance, 2022; Danda, 2021; Gharavi et al., 2021)).

Unfortunately, such two-stage procedures can lead to sub-optimal and hard-to-explain results (Chang, 1983), as the embedding ignores important clustered structure in the data, which may harm the embedding. Further, as the embedding is agnostic to the underlying clusters, it may not provide a good space in which to separate the clusters (see Fig. 1). These issues motivate a need for joint clustering and embedding for such data. Further, such concerns extend to multiple data sets (“multiview” problems), where clustering and embedding has also frequently been approached as a two-step process where a low-rank, multiview embedding is obtained first and then input into a clustering algorithm (e.g., canonical correlation analysis followed by clustering, a common approach: (Chen et al., 2008; Chen & Schizas, 2013; Drysdale et al., 2017; Du et al., 2017; Ouyang, 2019)).

In the area of joint clustering and embedding, a number of pioneering approaches have emerged, including cluster-aware feature selection (Wang & Allen, 2021), CCA mixture models (Fern et al., 2005; Lei et al., 2017), non-negative matrix factorization approaches (NMF) (Fogel et al., 2016; Wu & Ma, 2020; Zhou et al., 2021), and a variety of neural networks (e.g. (Huang et al., 2014; Wang et al., 2016; Yang et al., 2016; Mautz et al., 2020; Shin et al., 2020; Boubekki et al., 2021; Lakkis et al., 2021)). However, these approaches lack explainability as they rely on neural networks or complex formulations, prioritize clustering over interpretability, and perform poorly given limited data.

To develop an explainable and scalable formulation for joint clustering and embedding, we aimed to combine two

¹Department of Psychiatry and Brain and Mind Research Institute, Weill Cornell Medicine of Cornell University, New York, NY, USA ²<amb2022@med.cornell.edu> ³<col2004@med.cornell.edu>

Correspondence to:

Logan Groseknick <log4002@med.cornell.edu>

widely used and interpretable methods: principal components analysis (PCA) and hierarchical clustering. To do so in a tractable way, we turned to convex clustering. For the past decade, this convex approach to clustering has reinvigorated clustering research, providing both firm theoretical footing and yielding strong empirical results within the framework of convex optimization. Since initial work using sparse, structured convex penalties to encourage fusion of variables into clusters (Pelckmans et al., 2005; Hocking et al., 2011; Lindsten et al., 2011), there has been a flurry of theoretical and algorithmic improvements (Pan et al., 2013; Chi & Lange, 2015; Tan & Witten, 2015; Sui et al., 2018; Weylandt et al., 2020; Wang et al., 2020; Sun et al., 2021; Fodor et al., 2022). A desirable characteristic of the convex clustering approach is the simple convex penalty it uses to encourage clustering of the optimization variable, as this penalty can be readily incorporated into more complex problems. This has recently led to new approaches to biclustering (Allen et al., 2014; Chi & Lange, 2015), multi-view clustering (Wang & Allen, 2021), and supervised convex clustering (Wang et al., 2020).

To jointly fit PCA and cluster hierarchically, we exploit this flexibility and add a convex clustering penalty to the classical Frobenius loss formulation of the truncated singular value decomposition (tSVD) (Eckart & Young, 1936). This results in a simple formulation for joint hierarchical clustering and principal component embedding. Although nonconvex, the objective function consists of only the tSVD loss term and a convex penalty, allowing for rapid fitting to a path of hierarchical solutions. Further it is amenable to scalable optimization for fitting larger N than previously possible for convex clustering methods (while estimating within-cluster principal components).

As this method learns a smooth, continuous path of hierarchical clustering solutions as a penalty parameter (λ) is varied, we call it Pathwise Clustered Matrix Factorization (PCMF). The approach’s ability to cluster and fit principal components simultaneously allows it to handle the uncentered structure of different clusters while still yielding correct within-cluster loadings (Fig. 1g). It is explainable as it returns both a dendrogram describing the cluster structure and the principal component scores and loadings per-cluster. Importantly, it can also be extended to joint multiview (CCA) embedding and clustering highly relevant to current problems in multi-omics, animal research, and psychiatry.

2. Main Contributions and Significance

1. We introduce a method for joint hierarchical clustering and embedding (PCMF) that adds a convex clustering penalty to the tSVD to yield joint hierarchically clustering and principal components within each cluster (Fig.

- 1). This is significant, as it is a new and uniquely explainable (e.g., yielding per-cluster principal component loadings), sensitive (effective for small N /small clusters), and scalable (able to fit large N , e.g., $N = 100,000$) approach to joint embedding and clustering.
2. We present fast algorithms to solve PCMF and locally linear PCMF (LL-PCMF) problems along a path of solutions, accelerate them using Algorithmic Regularization (Weylandt et al., 2020), and introduce a consensus approach that scales them to much larger N than previously possible with convex clustering.
3. We introduce a method to recover a dendrogram from the PCMF and LL-PCMF clustered matrix approximations.
4. We generalize our method to multiview learning, introducing a novel approach and algorithm: Pathwise Clustered Canonical Correlation Analysis (P3CA/LL-P3CA).
5. We compare our approach to state-of-the-art methods on 15 real world data sets in both the limited data $p > N$ and large N regimes.

3. Related Work: Convex Clustering

Traditional clustering algorithms such as K-means or hierarchical clustering aim to partition observations into more homogeneous subsets and are traditionally formalized as discrete optimization problems that are NP-hard. By relaxing the hard clustering constraint to a convex penalty (Pelckmans et al., 2005), clustering can be reformulated as a convex optimization problem. In such “convex clustering” (also referred to as “clusterpath” or “sum-of-norms” clustering), the fitting procedure trades off approximating the data well with minimizing the sum of between-observation distances via a tuning penalty parameter, λ . The number of clusters is indirectly controlled by λ , and when solved along a path of λ s, convex clustering can exactly recover true data partitions among a mixture of Gaussians (Lindsten et al., 2011; Hocking et al., 2011; Jiang et al., 2020). Further, this path of clustering solutions can be used to visualize hierarchical structure among the clusters as a dendrogram (Weylandt et al., 2020).

More explicitly, for data matrix $X \in \mathbb{R}^{N \times p}$ with N observations in the rows and p variables in the columns, convex clustering solves the problem:

$$\underset{\hat{X} \in \mathbb{R}^{N \times p}}{\text{minimize}} \frac{1}{2} \|X - \hat{X}\|_F^2 + \lambda \sum_{i < j} w_{ij} \|\hat{X}_{i \cdot} - \hat{X}_{j \cdot}\|_q. \quad (1)$$

The problem takes a “Lagrangian” form, with the penalty parameter $\lambda > 0$ continuously trading off a relaxed clustering inequality constraint (the sum of convex q -norms of differences between observations—typically $q \in \{1, 2, \infty\}$) with model fit to the data. Without this penalty, the problem is highly overparameterized and every row (sample/observation) has its own centroid. Weights $w_{ij} > 0$ can

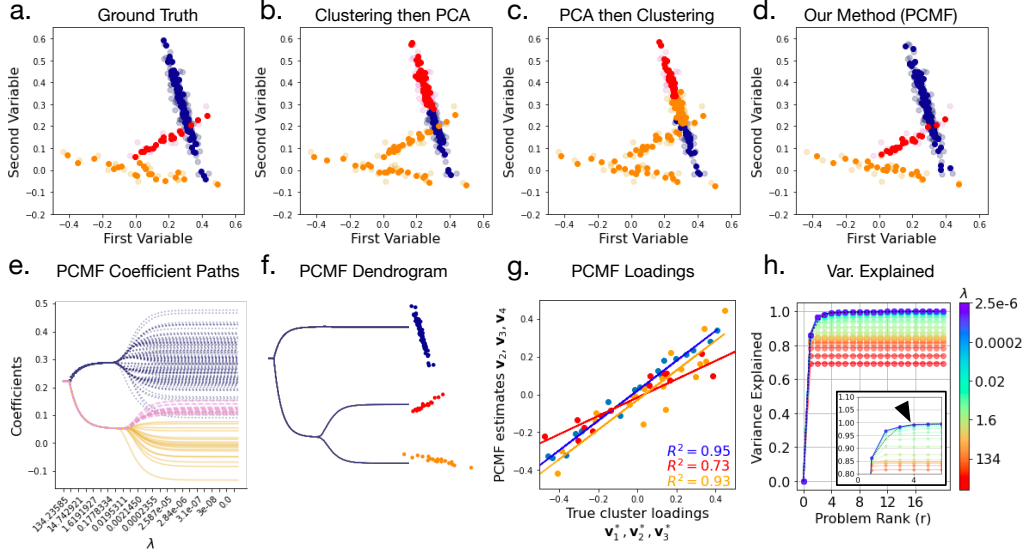


Figure 1: Explainable joint PCA and hierarchical clustering with PCMF. **a.** Ground truth data for 3-class problem; $p = 20$; $N_1 = 100$ (blue), $N_2 = 25$ (red), $N_3 = 25$ (orange). The first two variables of the data are plotted with light points showing raw data and dark points showing data reconstructed from low rank estimates, colored by true cluster membership (PCA rank $r = 4$). **b.** Spectral clustering sequentially followed by PCA on the clusters (rank $r = 4$; points colored by cluster membership estimates). **c.** PCA ($r = 4$) sequentially followed by Spectral Clustering on the principal components (points colored by cluster membership estimates). **d.** Our method (PCMF), which jointly estimates PCA and clusters (shown at $r = 4$; $\lambda = 3.0$; points colored by cluster membership estimate). Note both two-stage procedures fail to find the correct clusters while PCMF succeeds. **e.** PCMF coefficient paths for a variable fit along penalty path fit decreasing from $\lambda = \infty$ to $\lambda = 0$ (see Suppl. Movie 1 for an animation). **f.** Interpretable PCMF dendrogram estimated from the coefficient paths. **g.** PCMF loadings accurately and cluster-specifically fit the ground truth coefficients used to generate the data. PCMF loadings \mathbf{v}_2 , \mathbf{v}_3 , and \mathbf{v}_4 approximate true loadings \mathbf{v}_1^* , \mathbf{v}_2^* , and \mathbf{v}_3^* (shown in blue, red, and orange, respectively); \mathbf{v}_1 corresponds to the vector along which cluster means vary (not shown). **h.** Calculating variance explained by each PCMF component suggests a model with rank $r = 4$, (which correctly captures the 3 cluster slopes and the one dimensional direction along which the cluster means vary (arrow), see Appendix §B.2; dotted line shows standard PCA for comparison).

be added to increase the flexibility in modeling local structure in the row differences such as with a radial basis function ($w_{ij} = \exp(-\gamma \|X_i - X_j\|_2^2)$) (Hocking et al., 2011; Chi & Lange, 2015). However, multiplicative weights or properly scaling kernels may provide better theoretical guarantees (Jiang et al., 2020; Fodor et al., 2022). To speed up optimization and (sometimes significantly) improve results, weights may be constrained to only be nonzero for nearest neighbors (Chi & Lange, 2015; Wang & Allen, 2021).

Multiple algorithms have been proposed to solve agglomerative convex clustering including subgradient descent (Hocking et al., 2011), the stochastic incremental algorithm (Panahi et al., 2017), the semismooth Newton-CG augmented Lagrangian method (Sun et al., 2018), and primal-dual operator splitting methods using the Alternating Direction Method of Multipliers (ADMM) or the Alternating Minimization Algorithm (AMA) (Chi & Lange, 2015). Agglomerative convex clustering has been shown to converge and yield hierarchical dendrograms under certain satisfiable regularity conditions (Radchenko & Mukherjee, 2017; Chi

& Steinerberger, 2019; Weylandt et al., 2020). Recently, a warm-started ADMM approach—Algorithmic Regularization, which converges along a path of values of regularization penalty (λ)—has been shown to strongly converge to ADMM solutions; this enables feasible computation of dense convex clustering λ paths by increasing the speed in which the algorithm converges by > 100 times (Weylandt et al., 2020). Multiple studies have evaluated the statistical properties of convex optimization and its extension to clustering (Friedman et al., 2007; Boyd et al., 2011; Panahi et al., 2017; Chiquet et al., 2017; Sun et al., 2018; IEEE & Weylandt, 2019; Jiang et al., 2020; Lin & Chen, 2021), but none have explored using the convex clustering penalty for hierarchical clustering of PCA and CCA, as we do here. Convex biclustering (Chi et al., 2017) is perhaps the most similar in spirit, but significantly, it does not allow the same variables to contribute differentially to more than one cluster of observations, as our pathwise clustered PCA and CCA approaches do.

4. Pathwise Clustered Matrix Factorization (PCMF)

4.1. Problem Formulation

Consider a data matrix $X \in \mathbb{R}^{N \times p}$ with N observation in the rows and p variables in the columns, rank $R \leq \min(N, p)$, and without loss of generality assume X has been centered (see Appendix §B.2 for further discussion of uncentered effects). Among the most well-known and widely-employed algorithms is the truncated singular value decomposition (tSVD), where the rank- R reconstruction to X is given by $X = USV^T$, where $U^T U = I_N$, $V^T V = I_p$, $S = \text{diag}(s_1, \dots, s_r)$ and $s_1 \geq s_2 \geq \dots \geq s_r > 0$. It is a classic result (Eckart & Young, 1936) that for any $r \leq R$ the “truncated” SVD satisfies:

$$\hat{X} = U_r S_r V_r^T = \underset{\hat{X} \in M(r)}{\text{argmin}} \frac{1}{2} \|X - \hat{X}\|_F^2, \quad (2)$$

where $M(r)$ is the set of rank- $r \leq R$ matrices of N rows and p columns, U_r and V_r contain the first r left and right singular vectors in their respective columns, and S_r is square with the first r ordered singular values on its diagonal.

This decomposition is ubiquitously employed throughout statistics, engineering, and life sciences for dimensionality reduction, denoising, and data modeling. It is frequently used for capturing directions of maximum variance or covariance in data, as it is the algorithmic basis of principal components analysis (PCA), total least squares regression (TLS), and canonical correlation analysis (CCA).

We aim to generalize the tSVD to allow clustering among the observations, such that different clusters contain different variance-maximizing tSVD approximations. To do this we follow the convex clustering literature and augment (2) with the following sum-of-norms regularization (with $q \in \{1, 2, \infty\}$):

$$\underset{\hat{X} \in M(r)}{\text{minimize}} \frac{1}{2} \|X - \hat{X}\|_F^2 + \lambda \sum_{i < j} w_{ij} \|\hat{X}_i - \hat{X}_j\|_q. \quad (3)$$

Note that when $r = R$ (that is, if $\text{rank}(\hat{X}) = \text{rank}(X)$), this problem reduces to standard convex clustering (1). Expressing the matrix rank constraint $\hat{X} \in M(r)$ explicitly in terms of the tSVD, this optimization problem can be written:

$$\begin{aligned} & \underset{\hat{X}, U_r, S_r, V_r}{\text{minimize}} \frac{1}{2} \|X - \hat{X}\|_F^2 + \lambda \sum_{i < j} w_{ij} \|\hat{X}_i - \hat{X}_j\|_q \quad (4) \\ & \text{subject to } \hat{X} - U_r S_r V_r^T = 0, \quad U_r^T U_r = V_r^T V_r = I_r, \\ & S_r = \text{diag}(s_1, \dots, s_r), \end{aligned}$$

for $s_1 \geq s_2 \geq \dots \geq s_r > 0$, which can be interpreted as a convex clustering problem with truncated SVD constraints. We next present two algorithmic approaches to solving this problem.

4.2. Solving PCMF with ADMM

First, we present an approach solving PCMF with ADMM. Because in most cases it is desirable for many weights w_{ij} in the convex clustering penalty to be exactly zero (Chi & Lange, 2015), we can represent the relevant nonzero distances as a sparse graph G . We then introduce an auxiliary variable $G = D\hat{X} \in \mathbb{R}^{|\mathcal{E}| \times p}$, where $D \in \mathbb{R}^{|\mathcal{E}| \times n}$ is a sparse matrix containing the weighted pairwise distances defined by edges \mathcal{E} . This allows us to rewrite the PCMF problem as:

$$\begin{aligned} & \underset{\hat{X}, G, U_r, S_r, V_r}{\text{minimize}} \frac{1}{2} \|X - \hat{X}\|_F^2 + \lambda \sum_{\ell \in \mathcal{E}} w_\ell \|G_\ell\|_q \\ & \text{subject to } \hat{X} - U_r S_r V_r^T = 0, \quad G - D\hat{X} = 0, \\ & U^T U = V^T V = I_r, \quad S_r = \text{diag}(s_1, \dots, s_r), \end{aligned} \quad (5)$$

for $s_1 \geq \dots \geq s_r > 0$, which yields a problem separable in its objective and penalty subject to (nonconvex) constraints—a common application for ADMM. Algorithm 1 shows the ADMM updates, using Algorithmic Regularization (Weylandt et al., 2020) along the λ path. ADMM solutions fit along a path of λ s benefit from “warm-starting” by initializing the next problem along the path at the previous solution. Algorithmic Regularization takes this to the extreme, shortening steps along the path and decreasing the number of ADMM iterations at each point to a small number (achieved by making K small in Algorithm 1). For an appropriately chosen step size, this has been proven to converge to the true path solutions and speed up the computation of path estimation by > 100 times (Weylandt et al., 2020). Critically, this improves computational feasibility since the algorithm requires solving over many path parameter (λ) values (see Appendix for derivation, convergence details, and computational complexity).

4.3. Locally-Linear PCMF (LL-PCMF) with a Penalized Alternating Least Squares Relaxation

Second, we present a Penalized Alternating Least Squares (PALS) approach that, when relaxed, provides a locally linear embedding (Roweis & Saul, 2000) fitting of per-cluster factors. Without loss of generality, we consider the rank-1 version of this problem (which can be generalized to rank- r using an appropriate deflation approach; see Mackey (2008); Witten et al. (2009)). Denoting the i th column vector of X^T as $\mathbf{x}_i = (X^T)_i$ and defining penalty $\tilde{P}_{\mathbf{w}, q}(\mathbf{u}, \mathbf{v}) = \sum_{(i, j) \in \mathcal{E}} w_{ij} \|u_i \mathbf{v} - u_j \mathbf{v}\|_q$, we can write the rank-1 truncated SVD with a convex clustering penalty (see Appendix §E) as:

$$\begin{aligned} & \underset{s, \mathbf{u}, \mathbf{v}}{\text{minimize}} \sum_{i=1}^N \frac{1}{2} \|\mathbf{x}_i - s u_i \mathbf{v}\|_2^2 + \lambda \tilde{P}_{\mathbf{w}, q}(\mathbf{u}, \mathbf{v}) \quad (6) \\ & \text{subject to } \|\mathbf{u}\|_2^2 = 1, \quad \|\mathbf{v}\|_2^2 = 1, \quad s > 0. \end{aligned}$$

To introduce the overparameterization necessary for con-

Algorithm 1 PCMF

Input: data X , decreasing path $\{\lambda\}$, weights \mathbf{w} , pairwise distance matrix D

Notation: data mean \bar{X} , rank r , iteration k , norm $q \in \{1, 2, \infty\}$, $\rho \geq 1$, proximal operator $\text{prox}_{\frac{\lambda}{\rho} P_{\mathbf{w},q}(G)}$

- 1: $G^0 \leftarrow Z_1^0 \leftarrow DX$;
- $\hat{X} \leftarrow Z_2^0 \leftarrow \bar{X}$, $(U_r^0, S_r^0, V_r^0) \leftarrow \text{SVD}_r(\hat{X})$,
 $L = \text{chol}(I + \rho I + \rho D^T D)$
- 2: **for** $\lambda \in \{\lambda\}$ **do**
- 3: **for** $k = 1, \dots, K$ **do**
- 4: $\hat{X}^{k+1} \leftarrow L^{-T} L^{-1} (X + \rho D^T (G^k - Z_1^k) + \rho (U_r^k S_r^k V_r^{kT} - Z_2^k))$
- 5: $G^{k+1} \leftarrow \text{prox}_{\frac{\lambda}{\rho} P_{\mathbf{w},q}(G)} (D \hat{X}^{k+1} + Z_1^k)$
- 6: $(U_r^{k+1}, S_r^{k+1}, V_r^{k+1}) \leftarrow \text{SVD}_r(\hat{X}^{k+1} + Z_2^k)$
- 7: $Z_1^{k+1} \leftarrow Z_1^k + D^T \hat{X}^{k+1} - G^{k+1}$
- 8: $Z_2^{k+1} \leftarrow Z_2^k + \hat{X}^{k+1} - U_r^{k+1}, S_r^{k+1}, V_r^{k+1}$
- 9: **end for**
- 10: Save current path solutions: $\hat{X}_\lambda \leftarrow \hat{X}^K$, $G_\lambda \leftarrow G^K$,
 $(U_{r,\lambda}, S_{r,\lambda}, V_{r,\lambda}) \leftarrow (U_r^K, S_r^K, V_r^K)$
- 11: Initialize for next path solution: $\hat{X}^0 \leftarrow \hat{X}^K$,
 $G^0 \leftarrow G^K$, $(U_r^0, S_r^0, V_r^0) \leftarrow (U_r^K, S_r^K, V_r^K)$
- 12: **end for**
- 13: **return** pathwise solutions
 $\{\hat{X}_\lambda\}, \{G_\lambda\}, \{U_{r,\lambda}\}, \{S_{r,\lambda}\}, \{V_{r,\lambda}\}$

vex clustering (and without loss of generality) we center and scale X , set $s = 1$, and replace the single vector \mathbf{v} with a matrix $V \in \mathbb{R}^{p \times N}$ with column vectors $\mathbf{v}_i = V_{:,i}$ (denoting the the set of these column vectors as $\{\mathbf{v}\}_i$, $i = 1, \dots, N$)—this allows each observation to potentially be its own cluster in the limit $\lambda \rightarrow 0$. This is similar to the relaxation in convex clustering, but now also means the local nearest neighbor or kernel-based weights in the penalty now also impose locally linear weighting of the first data fidelity term in optimization problem (3). We define $P_{\mathbf{w},q}(\mathbf{u}, V) = \sum_{(i,j) \in \mathcal{E}} w_{ij} \|u_i \mathbf{v}_i - u_j \mathbf{v}_j\|_q$ and arrive at the overparameterized problem:

$$\begin{aligned} & \underset{\mathbf{u}, V}{\text{minimize}} \sum_{i=1}^N \frac{1}{2} \|\mathbf{x}_i - u_i \mathbf{v}_i\|_2^2 + \lambda P_{\mathbf{w},q}(\mathbf{u}, V) \\ & \text{subject to } \|\mathbf{u}\|_2^2 = 1, \|\mathbf{v}_i\|_2^2 = 1, i = 1, \dots, N. \end{aligned} \quad (7)$$

To decrease computation time and improve the flexibility of fitting per-cluster factors, we remove the cross terms in the penalty; we relax the problem formulation by replacing $P_{\mathbf{w},q}(\mathbf{u}, \mathbf{v})$ with $Q_{\mathbf{w},q}^{\mathbf{u}}(\mathbf{u}) = \sum_{(i,j) \in \mathcal{E}} w_{ij} |u_i - u_j|$ and $Q_{\mathbf{w},q}^V(V) = \sum_{(i,j) \in \mathcal{E}} w_{ij} \|\mathbf{v}_i - \mathbf{v}_j\|_q$. Next, using fixed values from iterate k , $y_{\mathbf{u},i}^k = \mathbf{x}_i^T \mathbf{v}_i^k$ and $\mathbf{y}_{\mathbf{v},i}^k = u_i^k \mathbf{x}_i$, we

can write iterative updates:

$$\mathbf{u}^{k+1} \leftarrow \underset{\mathbf{u}}{\text{argmin}} \sum_{i=1}^N \|y_{\mathbf{u},i}^k - u_i\|_2^2 + \lambda Q_{\mathbf{w},q}^{\mathbf{u}}(\mathbf{u}) \quad (9a)$$

$$\text{subject to } \|\mathbf{u}\|_2^2 = 1, i = 1, \dots, N,$$

$$\{\mathbf{v}_i\}^{k+1} \leftarrow \underset{\{\mathbf{v}_i\}}{\text{argmin}} \sum_{i=1}^N \|\mathbf{y}_{\mathbf{v},i}^k - \mathbf{v}_i\|_2^2 + \lambda Q_{\mathbf{w},q}^V(V)$$

$$\text{subject to } \|\mathbf{v}_i\|_2^2 = 1, i = 1, \dots, N.$$

(9b)

This results in the iterative updates each being standard convex clustering problems with added constraints. We will subsequently refer to a convex clustering solver as CONVEXCLUSTER. Here we implement our CONVEXCLUSTER as an ADMM algorithm that can be scaled using consensus ADMM (Appendix §G); however, other convex clustering solvers could be used instead. The CONVEXCLUSTER algorithm and further derivation of the LL-PCMF problem is given in the Appendix.

5. Pathwise Clustered CCA (P3CA)

We next extend PCMF to multiview learning, where we aim to learn the covariance structure between clustered observations measured using multiple data views (i.e., fitting canonical correlation analysis or CCA within clusters). To do so, we follow a derivation similar to LL-PCMF (note it is also straightforward to derive a linear P3CA by instead replacing the SVD with CCA in Alg. 1), we introduce the overparameterized pathwise clustered canonical correlation analysis (P3CA) optimization problem (recall $\mathbf{v}_i = V_{:,i}$ are column vectors of $V \in \mathbb{R}^{p \times N}$). We have data matrices $X \in \mathbb{R}^{N \times p_x}$, $Y \in \mathbb{R}^{N \times p_y}$ and variables $\mathbf{u}_i \in \mathbb{R}^{p_x}$, $\mathbf{v}_i \in \mathbb{R}^{p_y}$, and we define $\Sigma_i = X_i^T Y_i \in \mathbb{R}^{p_x \times p_y}$ and $Q_{\mathbf{w},q}(V) = \sum_{(i,j) \in \mathcal{E}} w_{ij} \|\mathbf{v}_i - \mathbf{v}_j\|_q$. This yields the problem:

$$\underset{\{\mathbf{u}_i\}, \{\mathbf{v}_i\}}{\text{maximize}} \sum_{i=1}^N \mathbf{u}_i^T \Sigma_i \mathbf{v}_i - \lambda Q_{\mathbf{w},q}(U) - \lambda Q_{\mathbf{w},q}(V) \quad (10)$$

$$\text{subject to } \|\mathbf{u}_i\|_2^2 = 1, \|\mathbf{v}_i\|_2^2 = 1,$$

for $i = 1, \dots, N$. Without inequality constraints, this is a biconvex problem in the $\{\mathbf{u}_i\}$ and $\{\mathbf{v}_i\}$ when the subproblems are relaxed by fixing $\tilde{\mathbf{x}}_i = \Sigma_i \mathbf{v}_i$ and $\tilde{\mathbf{y}}_i = \Sigma_i^T \mathbf{u}_i$ at each subiterate:

$$\{\mathbf{u}_i\}^{k+1} \leftarrow \underset{\{\mathbf{u}_i\}}{\text{argmin}} \sum_{i=1}^N \frac{1}{2} \|\tilde{\mathbf{x}}_i - \mathbf{u}_i\|_2^2 + \lambda Q_{\mathbf{w},q}(U)$$

$$\text{subject to } \|\mathbf{u}_i\|_2^2 = 1, i = 1, \dots, N,$$

(11a)

$$\{\mathbf{v}_i\}^{k+1} \leftarrow \underset{\{\mathbf{v}_i\}}{\operatorname{argmin}} \sum_{i=1}^N \frac{1}{2} \|\tilde{\mathbf{y}}_i - \mathbf{v}_i\|_2^2 + \lambda Q_{\mathbf{w},q}(V)$$

subject to $\|\mathbf{v}_i\|_2^2 = 1, i = 1, \dots, N.$ (11b)

Each update is a convex clustering problem, leading to Algorithm 2. Empirically, for sufficiently small steps sizes, Algorithmic Regularization closely approaches the ADMM solutions with a significant speed up (see Appendix §F–H).

Algorithm 2 Pathwise Clustered Canonical Correlation Analysis (P3CA)

Input: data (X, Y) , decreasing path $\{\lambda\}$, weights \mathbf{w} , norm $q \in \{1, 2, \infty\}$

Notation: iteration k , data means (\bar{X}, \bar{Y}) , $\mathbf{v}_i = V_i$, $\tilde{\mathbf{x}}_i = (\tilde{X}_i)^T, \tilde{\mathbf{y}}_i = (\tilde{Y}_i)^T, \rho \geq 1$

- 1: $U \leftarrow \bar{X}, V \leftarrow \bar{Y}$
 - 2: **for** $\lambda \in \{\lambda\}$ **do**
 - 3: **for** $k = 1, \dots, K$ **do**
 - 4: $\tilde{\mathbf{x}}_i^{k+1} \leftarrow \Sigma_i \mathbf{v}_i^k$ ($\Sigma_i = X_i Y_i^T \in \mathbb{R}^{p_X \times p_Y}$)
 for $i = 1, \dots, N$
 - 5: $\mathbf{u}_i^{k+\frac{1}{2}} \leftarrow \operatorname{CONVEXCLUSTER}(\tilde{X}^{k+1}, U^k, \lambda, \mathbf{w}, q)$
 - 6: $\mathbf{u}_i^{k+1} \leftarrow \operatorname{prox}_{\|\cdot\|_2}(\mathbf{u}_i^{k+\frac{1}{2}})$ for $i = 1, \dots, N$
 - 7: $\tilde{\mathbf{y}}_i^{k+1} \leftarrow \Sigma_i^T \mathbf{u}_i^{k+1}$ ($\Sigma_i^T = Y_i X_i^T \in \mathbb{R}^{p_Y \times p_X}$) for $i = 1, \dots, N$
 - 8: $\mathbf{v}_i^{k+\frac{1}{2}} \leftarrow \operatorname{CONVEXCLUSTER}(\tilde{Y}^{k+1}, V^k, \lambda, \mathbf{w}, q)$
 - 9: $\mathbf{v}_i^{k+1} \leftarrow \operatorname{prox}_{\|\cdot\|_2}(\mathbf{v}_i^{k+\frac{1}{2}})$ for $i = 1, \dots, N$
 - 10: **end for**
 - 11: Save path solutions: $U_i^K \leftarrow \mathbf{u}_i^{KT}; V_i^K \leftarrow \mathbf{v}_i^{KT}$ for $i = 1, \dots, N$; $(U_\lambda, V_\lambda) \leftarrow (U^K, V^K)$
 - 12: Initialize: $(U^0, V^0) \leftarrow (U^K, V^K)$
 - 13: **end for**
 - 14: **return pathwise solutions** $\{U_\lambda\}, \{V_\lambda\}$
-

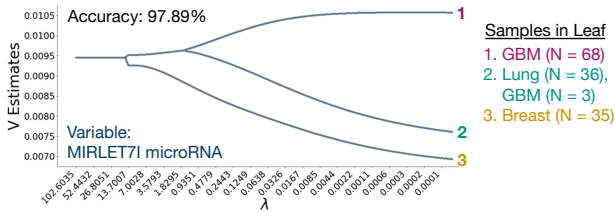


Figure 2: PCMF dendrogram on Tumors data shows cancer taxonomy with dendrogram splits consistent with observed confusion rate, highlighting interpretability.

6. Dendrograms and Model Selection

PCMF fits a path of solutions along a sequence of values of λ , and when using the ℓ_2 -norm ($q = 2$) (as we do for the remainder of the paper given its desirable rotational symmetry), not all members of a cluster are shrunk to exactly

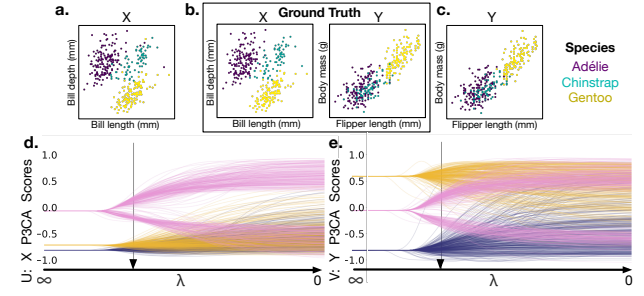


Figure 3: P3CA recovers 3 penguin species and identifies a hierarchy of shared embeddings (U on left and V on right). **a.** X variables colored by P3CA clustering solution indicated by the arrow. **b.** Ground truth clustering solution for X and Y variable sets. **c.** Y variables colored by best P3CA clustering solution indicated by the arrow. **d-e.** P3CA path diagrams for X and variable sets (colors indicate variable; pink is intercept term).

the same value (Hocking et al., 2011). Previous work has forced hard clustering at each agglomerative stage along the λ path (Hocking et al., 2011; Weylandt et al., 2020; Jiang et al., 2020). This may artificially force observations into one cluster that may then later switch to another, resulting in nonsmooth paths in practice. We choose to instead let the paths be unconstrained and smooth during solving, and then generate a dendrogram using a wrapper function that estimates sequential split points from the fully fit paths by sequentially testing whether increasing the number of clusters at each step would improve overall model fit in terms of the penalized log-likelihood. Clustering at each λ is performed on the weighted affinity matrix generated from differences matrix defined by the dual variables as recommended in (Chi & Lange, 2015). Thus this procedure estimates the connected components of the affinity graph defined by the dual variables at each value of λ . Further details on model selection are described in Appendix §J.

7. Experiments

7.1. Numerical Experiments and Real-World Data

We evaluate our methods in numerical experiments using synthetic data (Table 1 and Appendix Tables 4-5) and 15 real-world datasets (Table 1) dividing results into small underdetermined (limited observations $N, p > N$; Table 2) and large (many observations N ; Table 3). In Table 2 we measure clustering performance of PCMF against 3 classical (PCA+K-means, Ward, spectral, and DP-GMM) and 10 state-of-the-art (Elastic Subspace Clustering (You et al., 2016), gMADD (Sarkar & Ghosh, 2020; Paul et al., 2021), HDCC, Leiden, Louvain, DP-GMM, CARP) clustering methods including convex clustering (CARP) and 3 deep learning meth-

ods (DEC, IDEC, CarDEC) to accurately recover cluster labels in 18 synthetic datasets across 10 runs (Appendix Table 4) and in 15 real-world datasets (Tables 1-3). **Numerical Experiments.** We find that PCMF (solved with ADMM) and LL-PCMF (solved with PALS) with nearest neighbors $N.N. = 25$ performs competitively in 18 synthetic datasets, especially for $p > N$ ($p = 200, p = 2,000$; Appendix Table 4). **Cancer Subtype and Cell/Tissue Classification using Real-World Omic Datasets.** Finally, we evaluate our method on 15 (8 + 7 multiview partitions) real-world omic datasets and find PCMF outperforms 13 clustering methods (including CARP and state-of-the-art deep learning methods) in nearly all cases (except on the SRBCT data against DEC/IDEC; Table 2; Fig. 2). **Consensus Classification using Large Real-world and Synthetic Datasets.** We further show our consensus ADMM runs on larger N datasets (unlike standard convex clustering, which cannot run on $N > 1,000$) (Table 3) in real-world datasets ranging from $N = 400; p = 11,931$ to $N = 36,000; p = 784$ and a synthetic dataset of $N = 100,000; p = 1,000$. Further, in these larger datasets, we evaluate the generalization of our unsupervised PCMF algorithm to held-out test set data and find high held-out test set cluster assignment accuracy (see Appendix for details). To evaluate the PCA interpretation of PCMF embeddings, we compare and show high similarity to tSVD estimates on the ground-truth clusters (Fig. 1g and Appendix §B.2).

7.2. P3CA on Real-world Physiological, Omic, Behavioral, and Neuroimaging Datasets

We evaluate P3CA in six real-world datasets (Tables 1-2). **Species Classification.** First we apply P3CA to phenotypic data and classify penguin species with 98.25% accuracy (Horst et al., 2020) (Table 2 and Fig. 3).

Cancer Subtype and Cell/Tissue Classification using Real-World Omic Datasets. We evaluate P3CA on the same 4 complex real-world omic datasets as PCMF, but split the variables into X and Y (Table 1). We find P3CA outperforms or ties all 13 clustering methods (Table 2).

Predicting COVID-19 Severity. Using a COVID-19 dataset (Shen et al., 2020), we find P3CA identifies a metabolome-proteome embedding that predicts both COVID-19 severity and potential protein and metabolite biomarkers. P3CA recovers true patient severity subgroups (healthy, non-severe, severe) with the highest accuracy (91.11%) compared to other methods (Table 2). P3CA is successful on a very small sample of $N = 45$ subjects with $p \approx 400$ variables for each data view. By correlating the metabolome/proteome P3CA variate with metabolite/protein abundance, we identify severity-associated proteins and metabolites (Fig. 4). Importantly, the direction

of association can be shared across subgroups (SERPINA3 in Fig. 4a) or can differ across subgroups (see r -values for stachydrine in Fig. 4b)—an advantage of P3CA over standard canonical correlation analysis that can only capture shared associations across all subjects/samples. The associated proteins/metabolites to COVID-19 are supported by prior work: SERPINA3 (alpha-1 antichymotrypsin) is an immune marker in the coagulation/fibrinolytic cascade (Rubin et al., 1990) that has been associated with COVID-19 (Shen et al., 2020; D’Alessandro et al., 2020); stachydrine (alias proline betaine) is an osmotic protective agent/compound (Chambers & Kunin, 1987) associated with a number of medical disorders (Cheng et al., 2020), and osmotic crisis is a risk factor for severe COVID-19 (Muhanna et al., 2020).

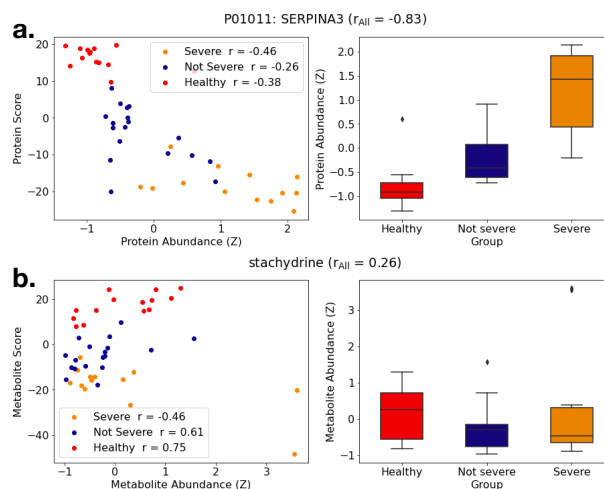


Figure 4: Associations between P3CA variates and protein / metabolite abundance predict COVID-19 severity. **a.** Proteome (X) P3CA variate is associated with SERPINA3 abundance. Right: Distribution of SERPINA3 abundance by patient group. **b.** Left: Metabolome (Y) P3CA variate is associated with stachydrine abundance, and strength/direction of association differs between groups. Right: Distribution of stachydrine abundance by patient group. r_{all} indicates correlation between all patients.

Discovery of Subtypes of Autism Spectrum Disorder (ASD). In Appendix §K.2 (Appendix Fig. 12 and Appendix Tables 6-7), we demonstrate deploying P3CA for subtype discovery, in which true biological subtypes are unknown but could inform diagnosis and the development of personalized treatments (Drysdale et al., 2017; Grosenick et al., 2019). P3CA identifies distinct biological subtypes of $N = 299$ ASD patients by finding a clustered CCA embedding of multivariate clinical behavior ($X = 3$) features and functional brain connectivity ($Y = 20$ top features) with stable subject-level U and V coefficients (cosine similarity: 0.93 ± 0.05 for U estimates and 0.97 ± 0.03 for V estimates; 10 subsamples 70% patients).

Table 1: Datasets in Tables 2-3 and cluster discovery analysis. See Appendix §K for more details.

Dataset	Variables (p)	Samples (N)	Classes
NCI	6, 830 genes (expression) (X)	64	13 cell types
SRBCT	2, 318 genes (expression) (X)	88	4 cancer diagnoses
Mouse	16, 944 genes (scRNA-seq) (X)	125	7 mouse organ types
Tumors	11, 931 expression/methylation (X)	142	3 cancer diagnoses
Tumors-Large	11, 931 expression/methylation (X)	400	3 cancer diagnoses
MNIST	784 image pixels from 28 x 28 pixel image (X)	36, 000	6 digit types
MNIST Fashion	784 image pixels from 28 x 28 pixel image (X)	36, 000	6 clothing types
Synthetic data	1, 000 synthetic variables; $\delta = 0.5$ (X)	100, 000	4 clusters
COVID-19 (Multiview)	403 metabolites (X); 382 proteins (Y)	45	3 severities
NCI (Multiview)	1, 000 genes (expression) (X); 100 genes (expression) (Y)	64	13 cell types
SRBCT (Multiview)	1, 000 genes (expression) (X); 100 genes (expression) (Y)	88	4 cancer diagnoses
Mouse (Multiview)	1, 000 genes (scRNA-seq) (X); 100 genes (scRNA-seq) (Y)	125	7 mouse organ types
Tumors (Multiview)	1, 000 genes (expression) (X); 100 genes (expression) (Y)	142	3 cancer diagnoses
Autism (ASD) (Multiview)	3 behaviors (X); 20 RSFC features (Y)	299	Unknown (discovery analysis)
Palmer Penguin (Multiview)	2 features (X); 2 features (Y)	342	3 penguin species

Table 2: Clustering accuracy on small real-world datasets (“MV” abbreviates “Multiview”).

	NCI	SRBCT	Mouse	Tumors	COVID-19	Penguins	NCI-MV	SRBCT-MV	Mouse-MV	Tumors-MV
PCMF	43.79%	51.8%	73.6%	92.25%	—	—	—	—	—	—
LL-PCMF	64.06%	55.42%	80.00%	97.89%	—	—	—	—	—	—
P3CA	—	—	—	—	91.11%	98.25%	56.25%	65.06%	63.20%	98.59%
PCA + K-means	39.06%	40.96%	45.60%	50.00%	—	—	—	—	—	—
CCA + K-means	—	—	—	—	51.11%	79.82%	31.25%	37.35%	27.20%	50.70%
Ward	56.25%	40.96%	46.40%	94.37%	68.89%	96.78%	51.56%	40.96%	30.40%	94.36%
Spectral	43.75%	43.37%	45.60%	93.66%	82.22%	96.78%	50.00%	43.37%	40.00%	93.66%
Elastic Subspace	59.38%	49.40%	73.60%	94.37%	51.11%	97.37%	48.43%	40.96%	52.00%	94.37%
gMADD	42.19%	46.99%	42.40%	72.54%	51.11%	67.25%	39.06%	44.58%	35.20%	58.45%
HDCC	59.38%	34.94%	29.60%	50.00%	40.00%	88.01%	51.50%	38.55%	29.60%	50.00%
Leiden	50.00%	46.99%	68.00%	71.12%	82.22%	40.06%	48.43%	46.99%	49.60%	71.13%
Louvain	42.19%	48.19%	76.00%	94.34%	82.22%	65.20%	45.31%	48.19%	60.80%	93.66%
DP-GMM	46.88%	43.37%	54.40%	85.92%	73.33%	68.42%	45.31%	44.58%	39.20%	92.96%
hCARP	43.75%	46.99%	36.00%	75.25%	71.11%	79.82%	34.37%	43.37%	30.40%	93.66%
DEC	45.31%	71.08%	46.40%	94.37%	86.67%	88.89%	54.69%	65.06%	33.60%	94.37%
IDEC	48.44%	67.47%	61.60%	92.96%	73.33%	—	—	—	—	—
CarDEC	51.56%	40.96%	75.20%	90.14%	84.44%	—	—	—	—	—

Table 3: Clustering accuracy (ACC) and time elapsed (TOC) for consensus PCMF on large datasets. (“X” indicates computationally infeasible to run. “T” indicates infeasible due to run time out.)

	Tumors-Large; $N = 400$		MNIST; $N = 36,000$		Fashion MNIST; $N = 36,000$		Synthetic; $N = 100,000$	
	ACC	ACC (hold-out)	ACC	ACC (hold-out)	ACC	ACC (hold-out)	ACC	ACC (hold-out)
PCMF	100.00%	100.00%	99.93%	88.33%	99.94%	81.41%	100.00%	100.00%
PCA + K-means	89.75%	100.00%	29.64%	29.64%	45.00%	45.48%	50.09%	50.00%
Ward	90.50%	n/a	—X—	n/a	—X—	n/a	—X—	n/a
Spectral	92.00%	n/a	—X—	n/a	—X—	n/a	—X—	n/a
gMADD	61.50%	n/a	—X—	n/a	—X—	n/a	—X—	n/a
Leiden	66.25%	n/a	60.62%	n/a	38.31%	n/a	10.88%	n/a
Louvain	72.25%	n/a	69.88%	n/a	42.26%	n/a	10.85%	n/a
DEC	99.25%	n/a	—T—	n/a	—T—	n/a	—T—	n/a
IDEC	86.50%	n/a	55.25%	n/a	48.98%	n/a	—T—	n/a

8. Conclusion

Here we have introduced linear and locally linear versions of Pathwise Clustered Matrix Factorization (PCMF) and its generalization to multiview data—Pathwise Clustered Canonical Correlation Analysis (P3CA)—both approaches that jointly hierarchically cluster and embed high dimensional data using a convex clustering penalty. These methods are significant, as they are uniquely explainable and effective for both small N and small cluster size as well

as for very large N problems. We present novel, accelerated, and scalable algorithms to solve these problems along a path of solutions and introduce a method to recover a dendrogram from the pathwise solutions. We then validate our approaches on numerous synthetic and 15 real-world datasets. Our results showed our methods to be highly competitive with state-of-the-art approaches in terms of both clustering accuracy and in terms of the enhanced explainability allowed by the hierarchical discovery of cluster-wise principal components or canonical variates.

References

- Allen, G. I., Grosenick, L., and Taylor, J. A generalized Least-Square matrix decomposition. *J. Am. Stat. Assoc.*, 109(505):145–159, January 2014.
- Bishop, J. R., Zhang, L., and Lizano, P. Inflammation subtypes and translating inflammation-related genetic findings in schizophrenia and related psychoses: A perspective on pathways for treatment stratification and novel therapies. *Harv. Rev. Psychiatry*, 30(1):59–70, February 2022.
- Bonacchi, R., Meani, A., Bassi, C., Pagani, E., Filippi, M., and Rocca, M. A. MRI-Based clustering of multiple sclerosis patients in the perspective of personalized medicine (3930). *Neurology*, 94(15 Supplement), April 2020.
- Boubekki, A., Kampffmeyer, M., Brefeld, U., and Jenssen, R. Joint optimization of an autoencoder for clustering and embedding. *Mach. Learn.*, 110(7):1901–1937, July 2021.
- Boyd, S., Parikh, N., and Chu, E. *Distributed Optimization and Statistical Learning Via the Alternating Direction Method of Multipliers*. Now Publishers Inc, 2011.
- Chambers, S. T. and Kunin, C. M. Isolation of glycine betaine and proline betaine from human urine. assessment of their role as osmoprotective agents for bacteria and the kidney. *J. Clin. Invest.*, 79(3):731–737, March 1987.
- Chang, W.-C. On using principal components before separating a mixture of two multivariate normal distributions. *J. R. Stat. Soc. Ser. C Appl. Stat.*, 32(3):267–275, 1983.
- Chen, C.-L., Gong, Y.-C., and Tian, Y.-J. KCK-Means: A clustering method based on kernel canonical correlation analysis. In *Computational Science – ICCS 2008*, pp. 995–1004. Springer Berlin Heidelberg, 2008.
- Chen, J. and Schizas, I. D. Distributed sparse canonical correlation analysis in clustering sensor data. In *2013 Asilomar Conference on Signals, Systems and Computers*, pp. 639–643, November 2013.
- Cheng, F., Zhou, Y., Wang, M., Guo, C., Cao, Z., Zhang, R., and Peng, C. A review of pharmacological and pharmacokinetic properties of stachydrine. *Pharmacol. Res.*, 155:104755, May 2020.
- Chi, E. C. and Lange, K. Splitting methods for convex clustering. *J. Comput. Graph. Stat.*, 24(4):994–1013, December 2015.
- Chi, E. C. and Steinerberger, S. Recovering trees with convex clustering. *SIAM JOURNAL ON MATHEMATICS OF DATA SCIENCE*, 1(3):383–407, 2019.
- Chi, E. C., Allen, G. I., and Baraniuk, R. G. Convex biclustering. *Biometrics*, 73(1):10–19, March 2017.
- Chiquet, J., Gutierrez, P., and Rigail, G. Fast tree inference with weighted fusion penalties. *J. Comput. Graph. Stat.*, 26(1):205–216, January 2017.
- Ciortan, M. and Defrance, M. GNN-based embedding for clustering scRNA-seq data. *Bioinformatics*, 2022.
- D’Alessandro, A., Thomas, T., Dzieciatkowska, M., Hill, R. C., Francis, R. O., Hudson, K. E., Zimring, J. C., Hod, E. A., Spitalnik, S. L., and Hansen, K. C. Serum proteomics in COVID-19 patients: Altered coagulation and complement status as a function of IL-6 level. *J. Proteome Res.*, 19(11):4417–4427, November 2020.
- Danda, S. *Identification of Cell Types in scRNA-seq Data via Enhanced Local Embedding and Clustering*. PhD thesis, University of Windsor, 2021.
- Drysdale, A. T., Grosenick, L., Downar, J., Dunlop, K., Mansouri, F., Meng, Y., Fetcho, R. N., Zebley, B., Oathes, D. J., Etkin, A., Schatzberg, A. F., Sudheimer, K., Keller, J., Mayberg, H. S., Gunning, F. M., Alexopoulos, G. S., Fox, M. D., Pascual-Leone, A., Voss, H. U., Casey, B. J., Dubin, M. J., and Liston, C. Resting-state connectivity biomarkers define neurophysiological subtypes of depression. *Nat. Med.*, 23(1):28–38, January 2017.
- Du, L., Liu, K., Zhang, T., Yao, X., Yan, J., Risacher, S. L., Han, J., Guo, L., Saykin, A. J., Shen, L., and Initiative, A. A Novel SCCA Approach via Truncated l_1 -norm and Truncated Group Lasso for Brain Imaging Genetics. *Bioinform Oxf Engl*, 2017.
- Eckart, C. and Young, G. The approximation of one matrix by another of lower rank. *Psychometrika*, 1(3):211–218, September 1936.
- Fern, X. Z., Brodley, C. E., and Friedl, M. A. *Correlation Clustering for Learning Mixtures of Canonical Correlation Models*, pp. 439–448. 2005. doi: 10.1137/1.9781611972757.39. URL <https://epubs.siam.org/doi/abs/10.1137/1.9781611972757.39>.
- Fodor, L., Jakovetić, D., Boberić Krstićev, D., and Škrbić, S. A parallel ADMM-based convex clustering method. *EURASIP J. Adv. Signal Process.*, 2022(1):1–33, November 2022.
- Fogel, P., Gaston-Mathé, Y., Hawkins, D., Fogel, F., Luta, G., and Young, S. S. Applications of a novel clustering approach using Non-Negative matrix factorization to environmental research in public health. *Int. J. Environ. Res. Public Health*, 13(5), May 2016.

- Friedman, J., Hastie, T., Höfling, H., and Tibshirani, R. Pathwise coordinate optimization. *AOAS*, 1(2):302–332, December 2007.
- Gharavi, E., Gu, A., Zheng, G., Smith, J. P., Cho, H. J., Zhang, A., Brown, D. E., and Sheffield, N. C. Embeddings of genomic region sets capture rich biological associations in lower dimensions. *Bioinformatics*, 37(23):4299–4306, December 2021.
- Grosenick, L., Shi, T. C., Gunning, F. M., Dubin, M. J., Downar, J., and Liston, C. Functional and optogenetic approaches to discovering stable Subtype-Specific circuit mechanisms in depression. *Biol Psychiatry Cogn Neurosci Neuroimaging*, 4(6):554–566, June 2019.
- Hocking, T. D., Joulin, A., Bach, F., and Vert, J.-P. Clusterpath an algorithm for clustering using convex fusion penalties. *Proceedings of the 28th International Conference on Machine Learning*, 2011.
- Horst, A. M., Hill, A. P., and Gorman, K. B. palmerpenquins: Palmer archipelago (antarctica) penguin data. *R package version 0.1.0*, 2020.
- Huang, P., Huang, Y., Wang, W., and Wang, L. Deep embedding network for clustering. *2014 22nd International Conference on Pattern Recognition*, pp. 1532–1537, 2014.
- IEEE and Weylandt, M. Splitting methods for convex bi-clustering and co-clustering. In *2019 IEEE DATA SCIENCE WORKSHOP (DSW)*, pp. 237–242, 2019.
- Jiang, T., Vavasis, S., and Zhai, C. W. Recovery of a mixture of gaussians by sum-of-norms clustering. *J. Mach. Learn. Res.*, 21(225):1–16, 2020.
- Lakkis, J., Wang, D., Zhang, Y., Hu, G., Wang, K., Pan, H., Ungar, L., Reilly, M. P., Li, X., and Li, M. A joint deep learning model enables simultaneous batch effect correction, denoising, and clustering in single-cell transcriptomics. *Genome Res.*, 31(10):1753–1766, October 2021.
- Lei, E., Miller, K., and Dubrawski, A. Learning mixtures of Multi-Output regression models by correlation clustering for Multi-View data. September 2017.
- Lin, Y. X. and Chen, S. C. A centroid Auto-Fused hierarchical fuzzy c-means clustering. *IEEE Trans. Fuzzy Syst.*, 29(7):2006–2017, 2021.
- Lindsten, F., Ohlsson, H., and Ljung, L. Clustering using sum-of-norms regularization: With application to particle filter output computation. In *2011 IEEE Statistical Signal Processing Workshop (SSP)*, pp. 201–204, June 2011.
- Mackey, L. W. Deflation methods for sparse pca. In *NIPS*, volume 21, pp. 1017–1024, 2008.
- Mautz, D., Plant, C., and Böhm, C. DeepECT: The deep embedded cluster tree. *Data Science and Engineering*, 5(4):419–432, December 2020.
- Muhanna, D., Arnipalli, S. R., Kumar, S. B., and Ziouzenkova, O. Osmotic adaptation by Na⁺-Dependent transporters and ACE2: Correlation with hemostatic crisis in COVID-19. *Biomedicine*, 8(11), October 2020.
- Ouyang, Q. *Canonical Correlation and Clustering for High Dimensional Data*. PhD thesis, McMaster University, 2019.
- Pan, W., Shen, X., and Liu, B. Cluster analysis: Unsupervised learning via supervised learning with a non-convex penalty. *J. Mach. Learn. Res.*, 14(7):1865, July 2013.
- Panahi, A., Dubhashi, D., Johansson, F. D., and Bhattacharyya, C. Clustering by sum of norms: Stochastic incremental algorithm, convergence and cluster recovery. In Precup, D. and Teh, Y. W. (eds.), *Proceedings of the 34th International Conference on Machine Learning*, volume 70 of *Proceedings of Machine Learning Research*, pp. 2769–2777. PMLR, 2017.
- Paul, B., De, S. K., and Ghosh, A. K. Some clustering-based exact distribution-free k-sample tests applicable to high dimension, low sample size data. *J. Multivar. Anal.*, pp. 104897, November 2021.
- Pelckmans, K., De Brabanter, J., Suykens, J. A. K., and De Moor, B. Convex clustering shrinkage. In *PASCAL Workshop on Statistics and Optimization of Clustering Workshop*, 2005.
- Qian, T., Zhu, S., and Hoshida, Y. Use of big data in drug development for precision medicine: an update. *Expert Review of Precision Medicine and Drug Development*, 4(3):189–200, May 2019.
- Radchenko, P. and Mukherjee, G. Convex clustering via l1 fusion penalization. *J. R. Stat. Soc. Series B Stat. Methodol.*, 79(5):1527–1546, November 2017.
- Roweis, S. T. and Saul, L. K. Nonlinear dimensionality reduction by locally linear embedding. *Science*, 290(5500):2323–2326, 2000.
- Rubin, H., Wang, Z. M., Nickbarg, E. B., McLarney, S., Naidoo, N., Schoenberger, O. L., Johnson, J. L., and Cooperman, B. S. Cloning, expression, purification, and biological activity of recombinant native and variant human alpha 1-antichymotrypsins. *J. Biol. Chem.*, 265(2):1199–1207, January 1990.
- Santos, C., Sanz-Pamplona, R., Nadal, E., Grasselli, J., Pernas, S., Dienstmann, R., Moreno, V., Taberero, J., and

- Salazar, R. Intrinsic cancer subtypes—next steps into personalized medicine. *Cell. Oncol.*, 38(1):3–16, February 2015.
- Sarkar, S. and Ghosh, A. K. On perfect clustering of high dimension, low sample size data. *IEEE Trans. Pattern Anal. Mach. Intell.*, 42(9):2257–2272, September 2020.
- Shen, B., Yi, X., Sun, Y., Bi, X., Du, J., Zhang, C., Quan, S., Zhang, F., Sun, R., Qian, L., Ge, W., Liu, W., Liang, S., Chen, H., Zhang, Y., Li, J., Xu, J., He, Z., Chen, B., Wang, J., Yan, H., Zheng, Y., Wang, D., Zhu, J., Kong, Z., Kang, Z., Liang, X., Ding, X., Ruan, G., Xiang, N., Cai, X., Gao, H., Li, L., Li, S., Xiao, Q., Lu, T., Zhu, Y., Liu, H., Chen, H., and Guo, T. Proteomic and metabolomic characterization of COVID-19 patient sera. *Cell*, 182(1):59–72.e15, July 2020.
- Shin, S.-J., Song, K., and Moon, I.-C. Hierarchically clustered representation learning. *AAAI*, 34(04):5776–5783, April 2020.
- Singh, A. and Pandey, B. A new intelligent medical decision support system based on enhanced hierarchical clustering and random decision forest for the classification of alcoholic liver damage, primary hepatoma, liver cirrhosis, and cholelithiasis. *J. Healthc. Eng.*, 2018:1469043, February 2018.
- Sørli, T., Perou, C. M., Tibshirani, R., Aas, T., Geisler, S., Johnsen, H., Hastie, T., Eisen, M. B., van de Rijn, M., Jeffrey, S. S., Thorsen, T., Quist, H., Matese, J. C., Brown, P. O., Botstein, D., Lønning, P. E., and Børresen-Dale, A.-L. Gene expression patterns of breast carcinomas distinguish tumor subclasses with clinical implications. *Proceedings of the National Academy of Sciences*, 98(19):10869–10874, 2001. doi: 10.1073/pnas.191367098. URL <https://www.pnas.org/content/98/19/10869>.
- Sui, X. L., Xu, L., Qian, X., and Liu, T. Convex clustering with metric learning. *Pattern Recognit.*, 81:575–584, September 2018.
- Sun, D., Toh, K.-C., and Yuan, Y. Convex clustering: Model, theoretical guarantee and efficient algorithm preprint. October 2018.
- Sun, D., Toh, K.-C., and Yuan, Y. Convex clustering: Model, theoretical guarantee and efficient algorithm. *J. Mach. Learn. Res.*, 22(9):1–32, 2021.
- Tan, K. M. and Witten, D. Statistical properties of convex clustering. *Electron J Stat*, 9(2):2324–2347, October 2015.
- Wang, M., Yao, T., and Allen, G. I. Supervised convex clustering. May 2020.
- Wang, M. J. and Allen, G. I. Integrative generalized convex clustering optimization and feature selection for mixed Multi-View data. *J. Mach. Learn. Res.*, 22, 2021.
- Wang, W., Arora, R., Livescu, K., and Bilmes, J. On deep Multi-View representation learning: Objectives and optimization. February 2016.
- Weylandt, M., Nagorski, J., and Allen, G. I. Dynamic visualization and fast computation for convex clustering via algorithmic regularization. *J. Comput. Graph. Stat.*, 29(1):87–96, 2020.
- Witten, D. M., Tibshirani, R., and Hastie, T. A penalized matrix decomposition, with applications to sparse principal components and canonical correlation analysis. *Biostatistics*, 10(3):515–534, July 2009.
- Wu, W. and Ma, X. Joint learning dimension reduction and clustering of single-cell RNA-sequencing data. *Bioinformatics*, 36(12):3825–3832, June 2020.
- Yang, J., Parikh, D., and Batra, D. Joint unsupervised learning of deep representations and image clusters. In *Proceedings of the IEEE conference on computer vision and pattern recognition*, pp. 5147–5156, 2016.
- You, C., Li, C.-G., Robinson, D. P., and Vidal, R. Oracle based active set algorithm for scalable elastic net subspace clustering. May 2016.
- Zhou, L., Du, G., Lü, K., and Wang, L. A network-based sparse and multi-manifold regularized multiple non-negative matrix factorization for multi-view clustering. *Expert Syst. Appl.*, 174:114783, July 2021.